Nanohole-Structured and Palladium-Embedded 3D Porous Graphene for Ultrahigh Hydrogen Storage and CO Oxidation Multifunctionalities

Rajesh Kumar,[†,§] Jung-Hwan Oh,[†,§] Hyun-Jun Kim,[†] Jung-Hwan Jung,[†] Chan-Ho Jung,[‡] Won G. Hong,[∥] Hae-Jin Kim,[∥] Jeong-Young Park,[*,‡] and Il-Kwon Oh[*,†]

[†]Graphene Research Center, KAIST Institute for the NanoCentury, Department of Mechanical Engineering, and [‡]Center for Nanomaterials and Chemical Reactions, Institute for Basic Science, Graduate School of Energy, Environment, Water and Sustainability, Korea Advanced Institute of Science and Technology (KAIST), 291 Daehak-ro, Yuseong-gu, Daejeon 305-338, South Korea and [∥]Nano-Bio Electron Microscopy Research Group, Korea Basic Science Institute, 169-148 Gwahak-ro, Yuseong-gu, Daejeon 305-806, Republic of Korea. [§]R. Kumar and J.-H. Oh contributed to this work equally.

ABSTRACT Atomic-scale defects on carbon nanostructures have been considered as detrimental factors and critical problems to be eliminated in order to fully utilize their intrinsic material properties such as ultrahigh mechanical stiffness and electrical conductivity. However, defects that can be intentionally controlled through chemical and physical treatments are reasonably expected to bring benefits in various practical engineering applications such as desalination thin membranes, photochemical catalysts, and energy storage materials. Herein, we report a defect-engineered self-assembly procedure to produce a three-dimensionally nanohole-structured and palladium-embedded porous graphene hetero-nanostructure having ultrahigh hydrogen storage and CO oxidation multifunctionalities. Under multistep microwave reactions, agglomerated palladium nanoparticles having diameters of ~10 nm produce physical nanoholes in the basal-plane structure of graphene sheets, while much smaller palladium nanoparticles are readily impregnated inside graphene layers and bonded on graphene surfaces. The present results show that the defect-engineered hetero-nanostructure has a ~5.4 wt % hydrogen storage capacity under 7.5 MPa and CO oxidation catalytic activity at 190 °C. The defect-laden graphene can be highly functionalized for multipurpose applications such as molecule absorption, electrochemical energy storage, and catalytic activity, resulting in a pathway to nanoengineering based on underlying atomic scale and physical defects.

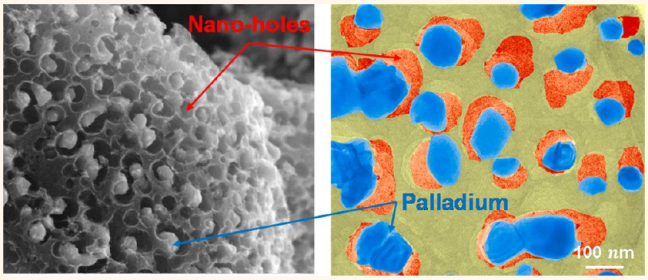

KEYWORDS: nanoholes · defect-laden graphene · CO oxidation · hydrogen storage · catalyst

During the past decade, two-dimensional (2D) crystalline nanomaterials including graphene, boron nitrite, chalcogenides, and metal−organic frameworks have been extensively investigated because they are expected to have exceptionally high intrinsic material properties and various engineering applications. However, atomic-scale defects observed in synthesized graphene and other carbon nanostructures can deteriorate these extraordinary mechanical, electrical, and chemical properties and delay the use of these materials in industrial applications. Therefore, innovative synthetic routes for producing high-quality nanostructures without atomic-scale defects, dislocations, or physical nanoholes should be further developed.

On the other hand, if atomic-scale defects or physical nanoholes in graphene and carbon nanostructures can be intentionally controlled or naturally self-assembled during the synthesis process, it will be possible to use the resulting materials in ultrathin desalination membranes, highly reactive catalysts, gas absorbents, and energy storage systems. Also, the defect sites can be more highly functionalized through chemical treatments for specific engineering applications in the fields of biology, medicine,

* Address correspondence to ikoh@kaist.ac.kr, jeongypark@kaist.ac.kr.

Received for review April 19, 2015 and accepted June 10, 2015.

Published online June 10, 2015
10.1021/acsnano.5b02337

environmental protection, catalysis, and energy storage and conversion. Controlled defects can be intentionally utilized as nucleation sites for graphene–metal hybrid materials and three-dimensional (3D) hetero-nanostructures combining nanoparticles, nanowires, nanotubes, and 2D sheets. Furthermore, defect-functionalized porous graphene along edge lines and on surfaces is required for engineering applications, such as chemical energy conversion and hydrogen storage. One of the most attractive features of 3D graphene–metal hybrids is that they can interact with various organic or inorganic species not only on the surface but also through their porous frameworks. These characteristics are very important in separation, gas storage, adsorption, and heterogeneous catalysis.[1−4] The fabrication of unconventional graphene-based 3D nanostructures with different textural and porous properties is therefore an appealing endeavor for material scientists.

Until now, however, the generation of edge defects and nanoholes on graphene surfaces has not been widely investigated for applications in hydrogen storage and CO oxidation. Among various possibilities, porous graphene is recognized as a carbon-based adsorbent with large surface area and light weight, making substantial volumetric and gravimetric contents possible.[5−7] Furthermore, the storage capacity of graphitic nanomaterials (*e.g.*, graphene, carbon nanotubes, and fullerenes) can be significantly enhanced by decorating them with metal atoms that absorb multiple H_2 molecules *via* Kubas interactions.[8−11] Additionally, the tendency of metal atoms to cluster leads to a considerable reduction of the potential storage capacity.[12] In contrast, a metal cluster supported on a graphitic material acts as a catalyst and enhances the hydrogen uptake of the substrate *via* a spillover mechanism.[13,14] The hydrogen spillover technique has been suggested as an effective approach for enhancing hydrogen storage in porous graphene-based adsorbents. Many investigators have reported carbon-based adsorbents doped with metal nanoparticles (*e.g.*, Pt, Pd, and Ni) that resulted in increased hydrogen storage *via* the spillover phenomenon.[15,16]

A small amount of catalyst that is physically mixed as a spillover source with secondary adsorbents also enhances hydrogen storage on adsorbents; this strategy is defined as "secondary spillover".[17,18] The advantages of this technique are that it reduces the total weight of the noble metal, it allows individual preparation of the catalyst (source) and adsorbents (receptors), it maintains the nature of the receptor porosity, and it is suitable for practical manufacturing. The complete oxidation of carbon monoxide and gaseous hydrocarbons to carbon dioxide and water by catalysis is used to treat car exhaust, odors, and toxic gases.[19,20] Catalysts containing noble metals (*e.g.*, Au, Pt, and Pd) provide high activity and stability for carbon monoxide oxidation.

Herein, we report a defect-engineered self-assembly process for nanohole-structured and palladium-embedded 3D porous graphene (3D Pd-E-PG) that is specially designed for ultrahigh hydrogen storage and CO oxidation multifunctionalities. This synthetic route, which includes microwave irradiation, is very suitable for one-pot and fast mass production of a 3D Pd-E-PG hetero-nanostructure having highly activated nanoholes in the basal plane of the graphene surfaces. Nanosized Pd nanoparticles under low-power microwave radiation diffuse inside graphene layers and are anchored to the atomic-scale functional groups of graphene oxide surfaces. When high-power microwave radiation is applied as a following step, agglomerated Pd nanoparticles with much larger diameter (over ~10 nm) produce physical nanoholes on the graphene sheets and are finally embedded in the few-layered graphene. The carbon atoms along the edges of these nanoholes have unsaturated bonds; these unsaturated carbon bonds are highly reactive for hydrogen storage and CO oxidation. We have also studied the hydrogen storage and CO oxidation performance of 3D Pd-E-PG, palladium-decorated graphene (Pd-D-G), and microwave-exfoliated graphene oxide samples.

RESULTS AND DISCUSSION

We propose a mechanism for nanohole generation in 3D Pd-E-PG. The creation of nanoholes and Pd nanoparticles embedded in the graphene sheets is schematically illustrated in Figure 1. Microwaves work by directly coupling with polar molecules in a material, thus causing the particles to move and rotate, which in turn generates heat. Step I shows pristine microwave-exfoliated graphene oxide (MEGO), which contains a layered structure after the graphite oxide was exposed to microwave irradiation. It is well known that carboxyl, hydroxyl, and epoxy groups are three major functional groups on the surface of MEGO. The MEGO is then mixed with palladium acetate and ethanol to make a homogeneous catalyst. In step II, the pristine MEGO and palladium acetate [$Pd(O_2CCH_3)_2$] are mixed in C_2H_5OH for 3 h with the help of magnetic stirring. After drying this sample in an oven at 60 °C (*i.e.*, after complete evaporation of the C_2H_5OH), it becomes a powder, which is then treated with low-power microwave irradiation at 700 W for 30 s. During the microwave irradiation process, [$Pd(O_2CCH_3)_2$] decomposes into Pd nanoparticles, and these small Pd nanoparticles start to deposit on the graphene surface through attachment to oxygen functional groups. Under short-duration and low-power microwave irradiation, these nanoparticles are decorated on the graphene surfaces, resulting in Pd-D-G. These initially decorated Pd nanoparticles in Pd-D-G are isolated,

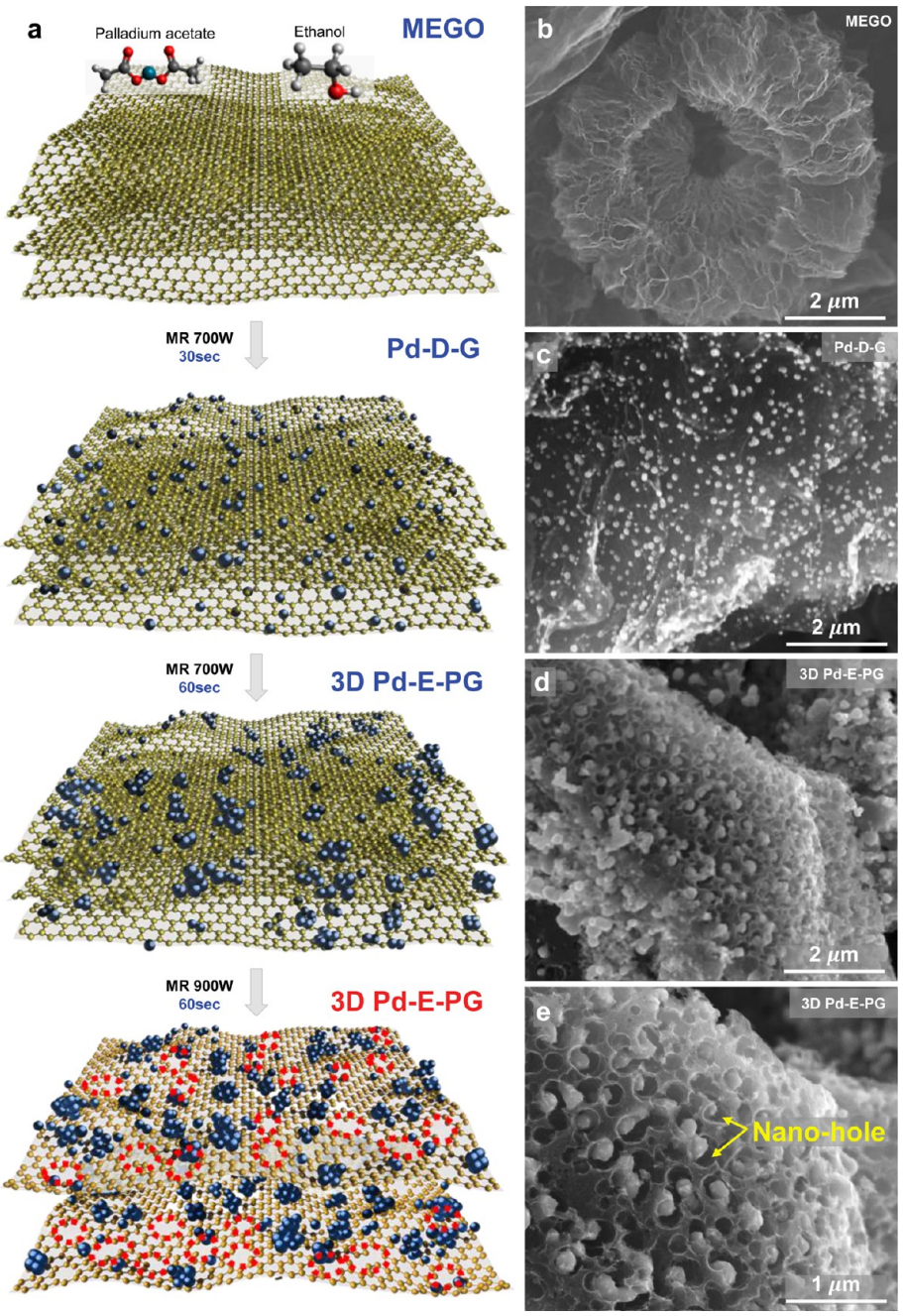

Figure 1. Synthesis route of nanohole-structured and palladium-embedded 3D porous graphene (3D Pd-E-PG) and corresponding SEM images. (a) Schematic illustration of the microwave fabrication process of the 3D Pd-E-PG. (b) SEM image of microwave-exfoliated graphene oxide. (c) SEM image of the uniform decoration of Pd nanoparticles on graphene layers after low-power microwave irradiation. (d) SEM image of the aggregation of Pd nanoparticles after successive high-power microwave irradiation. (e) SEM image of nanohole generation and the perforated graphene structures after multistep microwave irradiation.

ultrafine, and homogeneously distributed on the surface due to strong interactions between the Pd nanoparticles and the functional groups of MEGO. In step III, the previous Pd-D-G sample was microwave-irradiated for a long time (60 s); it was then observed that some Pd nanoparticles started to agglomerate on the graphene surface and that their diameter increased to ~10 nm. Step IV shows that these agglomerated Pd nanoparticles in Pd-D-G started to diffuse inside and to make nanoholes from the outer layers of the few-layered graphene during high-power microwave irradiation with an intensity of 900 W for 60 s. Under high-power microwave irradiation, the Pd nanoparticles reached high temperatures in a short time and started to penetrate into the few-layered MEGO along the *c*-axis. The agglomerated Pd nanoparticles, which have much larger diameters of over 10 nm, are clearly embedded, but smaller Pd nanoparticles remain on

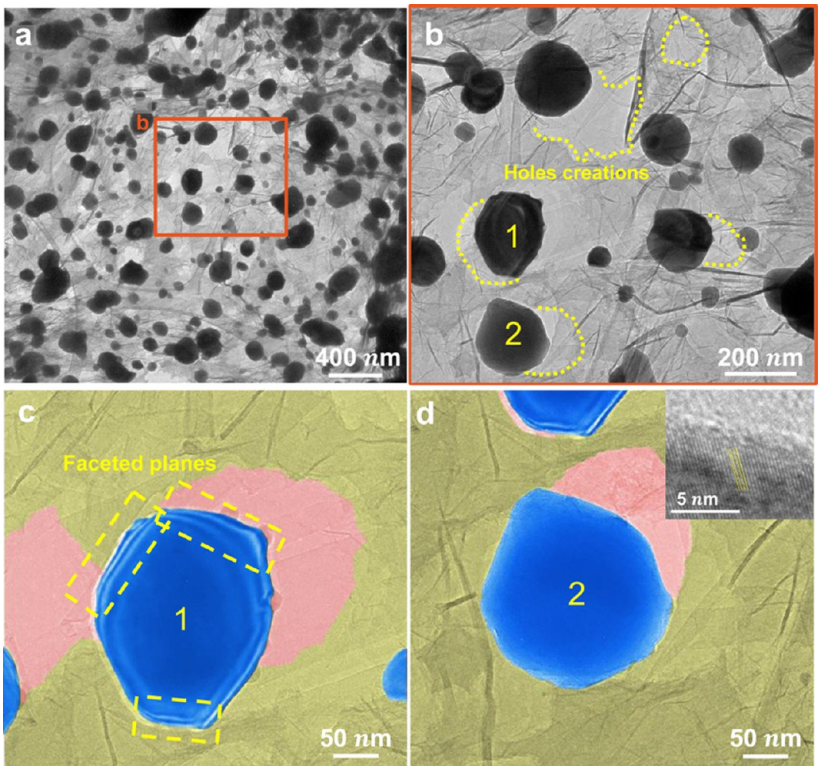

Figure 2. Transmission electron microscopy (TEM) images of 3D Pd-E-PG having nanoholes on graphene sheets and embedded Pd nanoparticles. (a) TEM image of the 3D Pd-E-PG. The nanoholes created by the Pd nanoparticles are observed on an amorphous graphene layer. The small colored box is the field of view for (b), the zoomed-in image of the box in (a), showing created holes. (c, d) Magnified TEM images around Pd nanoparticles in different areas. The inset shows the lattice planes of the Pd in (d).

the surface of the MEGO. The larger Pd nanoparticles produce nanoholes in the graphene surface, as shown in Figure 1. After longer duration microwave irradiation, the nanoholes containing Pd nanoparticles show high stability without detachment of the Pd particles from the 3D structures. The film growth mechanism in the metal deposition process on a substrate, in which the cohesive bonds between metal (Pd) atoms are stronger than the adhesive bonds between the Pd atoms and the MEGO, is well understood. It is worth noting in this instance that the surface energy of graphene is quite low, and thus the Pd nanoparticles are effectively embedded in the graphene surface.

The SEM images in Figure 1 were taken to investigate the surface morphologies of the samples through the step-by-step process, from MEGO to two-dimensional Pd-D-G to 3D Pd-E-PG. Figure 1b shows the MEGO containing porous, wrinkled, and fluffy stacked graphene microstructures due to microwave expansion of the graphite oxide along the *c*-axis. Figure 1c shows a Pd nanoparticle in contact with the MEGO support; the contact between the Pd nanoparticles and the MEGO appears to be quite uniformly distributed. The synthesis of Pd-D-G nanostructures is easily controlled by varying the microwave irradiation time and power. The graphene surfaces are completely covered by Pd nanoparticles. After increasing the microwave irradiation time, the creation of nanoholes inside the graphene layers using Pd nanoparticles leads to the creation of 3D Pd-E-PG nanostructures, as shown in Figure 1d. These Pd nanoparticles coalesced and formed nearly spherical aggregations on the graphene surface under longer (60 s) microwave irradiation. Some smaller Pd nanoparticles formed a larger spherical structure with an increased diameter as the irradiation time increased. The 3D Pd-E-PG clearly shows a perforated graphene surface with a uniform and unique morphology. The surface of the MEGO has pore-like structures ranging from 10 to 100 nm in diameter; the average aggregated Pd nanoparticles diffuse and are embedded into the graphene layers.

Typical TEM and HR-TEM images of the 3D Pd-E-PG are provided in Figure 2. The graphene sheet in the 3D Pd-E-PG has transparent flakes with a diameter of several micrometers. Corrugation and scrolling are part of the intrinsic nature of graphene sheets; these processes originate from the thermodynamic stability of the 2D graphene structure during bending. The TEM images show that the Pd nanoparticles create defects in the local surfaces of the MEGO. Figure 2b shows a higher magnification of the 3D Pd-E-PG, in which Pd nanoparticles show certain facet-like structures with various morphologies. HR-TEM analysis was carried out to further characterize the microstructures, as shown in

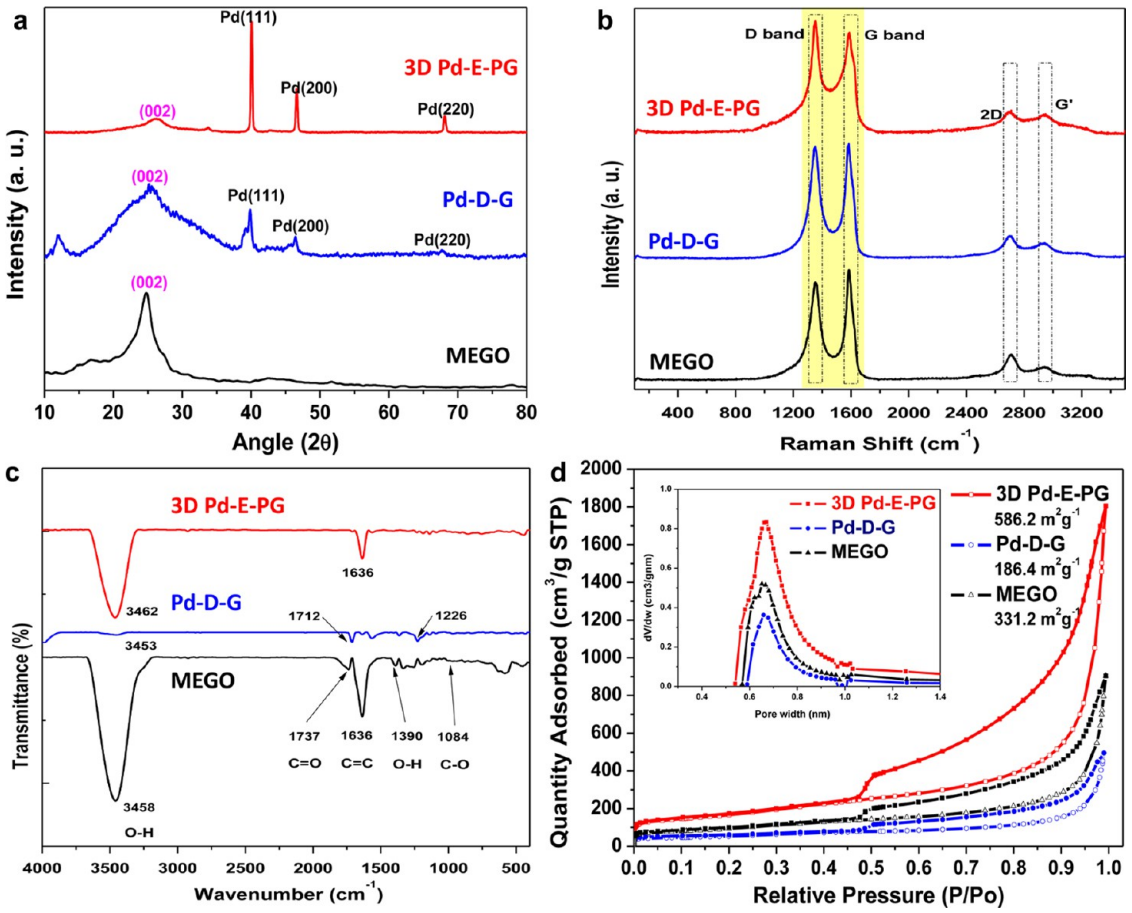

Figure 3. Structural and chemical characterization of 3D Pd-E-PG. (a) Powder X-ray diffraction pattern, (b) Raman spectra, (c) FT-IR spectra, and (d) BET analysis with average micropore size (at 77 K) of the MEGO, Pd-D-G, and 3D Pd-E-PG.

Figure 2c and d. The higher magnification of the HR-TEM image in Figure 2d (inset) clearly reveals the lattice planes of Pd, indicating its polycrystalline nature. The HR-TEM images of the Pd nanoparticles show that the spacing of the lattice fringe is 0.225 nm, which corresponds to the Pd (111) crystalline planes.[21]

The crystalline characteristics of the MEGO, Pd-D-G, and 3D Pd-E-PG were investigated using X-ray diffraction (XRD). In Figure 3a, both Pd-D-G and 3D Pd-E-PG have three sharp peaks at $2\theta = 40.44$, 46.95, and 68.73; these peaks correspond to the (111), (200), and (220) plane reflections of palladium, respectively, as provided by the International Center for Diffraction Data (JCPDS 01-087-0645) for Pd.[22] These peaks reveal the face-centered cubic (fcc) nature of the Pd nanoparticles. The peaks corresponding to Pd in the 3D Pd-E-PG are more intense than those in the Pd-D-G; this is because highly crystalline Pd nanoparticles are embedded in the 3D Pd-E-PG. The strongest peak appeared at $2\theta = 40.44$, showing that the Pd nanoparticles were embedded into the graphene sheets in the dominant (111)-oriented plane. In our XRD observations, the broader (002) peak of the MEGO appears at $2\theta = 24$, indicating that graphene sheets are restacked in the Pd-embedded graphene.

We can better understand the structural changes of graphene by investigating the Raman spectra.[23] The Raman spectra of the MEGO, Pd-D-G, and 3D Pd-E-PG (Figure 3b) include G peaks at 1588, 1587, and 1590 cm^{-1}, corresponding to first-order scattering of the E_{2g} mode. The G peak shifted to 1590 cm^{-1} in the 3D Pd-E-PG, indicating disorder or strain in the MEGO. The intensity of the G band in the 3D Pd-E-PG was reduced, compared with those in the MEGO (I_D/I_G = 0.89) and Pd-D-G (I_D/I_G = 1.09). The I_D/I_G ratios increase from 0.89 to 1.09 when Pd nanoparticles are embedded in the MEGO; this is due to the creation of local nanoholes on the graphene surface. Raman spectra of the 3D Pd-E-PG also show a prominent D peak at 1332 cm^{-1} and 2D peak at 2676 cm^{-1}; these peaks are due to increased physical defects caused by nanohole generation, which results in a significant increase in the D peak and a decrease in the 2D peak.[24]

A Fourier transform infrared spectrophotometer (FT-IR) was used to indicate degrees of decoration and agglomeration of the 3D Pd-E-PG during the fabrication process. Figure 3c shows the FT-IR transmittance spectra for the MEGO, Pd-D-PG, and 3D Pd-E-PG. The spectrum of the MEGO shows adsorption bands corresponding to C═O carbonyl stretching at

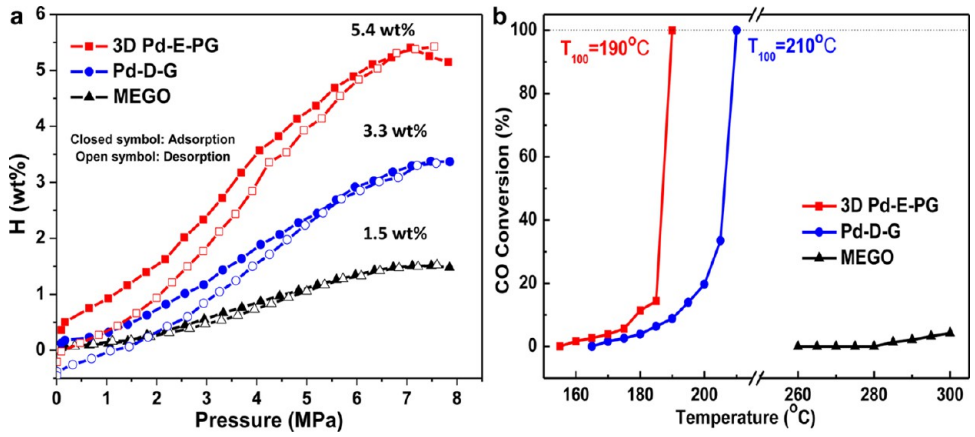

Figure 4. Multifunctional applications of 3D Pd-E-PG to hydrogen storage and CO oxidation catalyst. (a) High-pressure H_2 uptake at 77 K. (b) CO oxidation results showing the higher catalytic activity of 3D Pd-E-PG, compared to that of Pd-D-G. The MEGO is catalytically inert, exhibiting low conversion (less than 10% at 300 °C).

1737 cm^{-1}, O−H bending at 1390 cm^{-1}, and C−O stretching at 1084 cm^{-1}. The peaks at 1712 and 1226 cm^{-1} are attributed to the C═O and −OH of the −COOH groups, respectively, in the Pd-D-PG. Microwave-exfoliated graphene oxide is in the partially reduced state. In the synthetic process of MEGO, microwave radiation will remove oxygen functional groups of GO. Also, multiple microwave radiation steps for the synthesis of 3D Pd-E-PG will further reduce the oxygen functional groups. The C═O vibration band of MEGO decreases at ∼1737 cm^{-1} after the microwave-assisted reduction, indicating the partial reduction of GO, and this peak disappears in Pd-D-G and 3D Pd-E-PG as a result of remarkable reduction after the microwave treatment. We suppose that the influence of the reduction on the material characteristics and H2 absorption performance is minor, because I_D/I_G in the Raman spectra does not change significantly during the multiple microwave radiation steps, as shown in Figure 3b. The peak intensities of the functional groups are also reduced, indicating the decoration of Pd nanoparticles on the functional groups. The peak at 3453 cm^{-1} can be assigned to the Pd nanoparticles attached to the MEGO *via* oxygen-containing functional groups. After the multistep microwave irradiation, the adsorption bands of the oxygen functionalities mostly disappear and only the O−H stretching and C═C stretching bands remain, thus providing evidence of the agglomeration of Pd nanoparticles and the generation of nanoholes. From the experimental phenomena, we speculate that the Pd nanoparticles create defects as reactive sites that allow H atoms to be attached along the edge of nanoholes. These results were also confirmed *via* Raman spectra (Figure 3b) and XPS (Figure S1).

The Brunauer−Emmett−Teller (BET) specific surface areas of the MEGO, Pd-D-G, and 3D Pd-E-PG were measured from the nitrogen adsorption−desorption isotherms at 77 K, shown in Figure 3d; Table S1 presents a detailed study of the as-synthesized samples. The nitrogen adsorption−desorption isotherms of the 3D Pd-E-PG are type-IV adsorption isotherms. The presence of hysteresis in the isotherm signifies irreversible desorption, which is usually observed in specimens with a micropore structure (size <2 nm). The BET specific surface area of the 3D Pd-E-PG is measured as 586.2 $m^2\ g^{-1}$, while those of the Pd-D-G and the MEGO are 186.4 and 331.2 $m^2\ g^{-1}$, respectively. The inset in Figure 3d shows the pore size distribution of the MEGO, Pd-D-G, and 3D Pd-E-PG nanostructures using the H−K model. The 3D Pd-E-PG sample exhibits a microporous volume of 2.586 $cm^3\ g^{-1}$ with an average pore radius of 0.75 nm (inset of Figure 3d). This shows some peak intensity variation; the increase in the peak intensity for the 3D Pd-E-PG is due to the creation of nanoholes inside the graphene layers as a result of perforation of the graphene by the Pd nanoparticles and embedding of Pd nanoparticles in the graphene layers along the *c*-axis.

Figure 4a shows the high-pressure H_2 isotherms of the MEGO, Pd-D-G, and 3D Pd-E-PG at 77 K (up to 8 MPa). The maximum amounts of H_2 uptake of the MEGO, Pd-D-G, and 3D Pd-E-PG samples are 1.5, 3.3, and 5.4 wt %, respectively. It was observed that the 3D Pd-E-PG nanostructure shows the highest hydrogen adsorption in comparison with the MEGO and the Pd-D-G nanostructures. It is noted that the presence of oxygen functional groups and Pd carbonaceous materials increase the binding energies of spillover H and the hydrogen adsorption on the surface of carbonaceous materials. In the Pd-D-G and 3D Pd-E-PG samples, the Pd nanoparticles act as a catalyst to dissociate the H_2 molecule into H atoms effectively. There is a possibility that these dissociated H atoms will migrate to the MEGO surface when the H_2 molecules are chemisorbed on the dispersed Pd nanoparticles. Although the surface area of Pd-D-G is smaller than that of the MEGO, the H_2 uptake of the Pd-D-G increased compared to

that of the MEGO. The increase of H_2 uptake in Pd-D-G can be tentatively attributed to the hydrogen spillover effect.[25,26] Interestingly, however, a maximum H_2 uptake of ~5.4 wt % was achieved by 3D Pd-E-PG. This finding suggests that other factors are involved in the dramatic increase of hydrogen adsorption capability. Bonding between the MEGO catalyst support and the Pd nanoparticles plays a major role in the dissociation and migration of H_2 molecules. Thermodynamic spillover can occur from both free-standing and receptor-supported clusters. The oxygen-containing functional groups and defect-containing nanoholes in the 3D Pd-E-PG can be possible sites for spillover H uptake.[27,28] The Pd-D-G has atomic-scale defects on graphene surfaces within subnanometer, while the 3D Pd-E-PG has much larger physical defects with 1−100 nm diameters. In the Pd-D-G, the atomic-scale defects, which originated from oxygen functional groups of MEGO, will not be so reactive for the hydrogen storage and CO oxidation. However, in the 3D-E-PG, the physical nanoholes that are produced by Pd nanoparticles will be more reactive sites, which will allow H atoms to be attached along the edges of the nanoholes. In the Pd-D-G case, there are no nanohole-like defects on the graphene surface and all of the Pd nanoparticles are simply anchored only on the graphene sheets. These graphene-supported Pd nanoparticles help the spillover mechanism, and thus H_2 molecules dissociate into H atoms and adsorb only on the graphene surfaces. In the 3D Pd-E-PG sample, after spillover occurs, these H atoms reach the surface of the graphene and diffuse into the interlayer space further through the nanohole, and they are trapped either by physisorption or chemisorption at defect sites, heteroatoms, or oxygen functionalities. The nanohole edges have very high defect levels inside the graphene layers, and these carbon-containing edges have unsaturated bonds. The H atoms attach to this unsaturated carbon, which leads to enhance hydrogen storage. The nanoholes inside the graphene have unsaturated carbon bonds that can trap H atoms to complete the carbon vacancies. The overall mechanism is called spillover; it enhances the hydrogen storage capacity of the samples. The metal catalyst plays the central role by separating hydrogen atoms from each other and spilling them onto a graphene receptor.

Figure 4b shows the results of CO oxidation for the MEGO, Pd-D-G, and 3D Pd-E-PG. The temperature at 100% CO conversion (T_{100}) was 210 °C for Pd on the graphene surface (Pd-D-G) and 190 °C for Pd on nanoholes in the graphene (3D Pd-E-PG), indicating that the Pd with nanoholes in the graphene is catalytically reactive. The loadings of Pd-D-G and 3D Pd-E-PG are 13.3% and 24.9%, respectively. The CO conversion rates dramatically increase from 30% to 100%, and this is related to CO oxidation ignition. During ignition, the high rate of CO_2 production causes a rapid increase in temperature. The pristine graphene sample could not reach 100% CO conversion until 300 °C, thus demonstrating the lower catalytic activity of graphene-based materials. The activation energy, obtained from the Arrhenius plot of the MEGO, is 46.8 kcal/mol, which is much higher than those of the Pd-D-G (34.6 kcal/mol) and 3D Pd-E-PG (34.1 kcal/mol). This indicates that the reaction mechanism on pristine graphene is different from those of Pd-D-G and 3D Pd-E-PG due to the presence of Pd nanoparticles in these two materials. Catalytic activity of the Pd-D-G is close to that of Pd/ZnO nanoparticle catalysts (with a loading of 10%) synthesized by microwave irradiation, which showed a value of T_{100} at 194 °C. The higher catalytic activity of the 3D Pd-E-PG, compared with that of the Pd-D-G, is associated with the defective nature of the holes of the graphene that is catalytically more reactive than pristine graphene. This result suggests that the interface area of the Pd nanoparticles and the graphene edge sites can act as an active site under CO oxidation.[27,28]

Figure 5 shows the hydrogen uptake mechanism in the 3D Pd-E-PG nanoholes, in which Pd nanoparticles are embedded in the graphene sheets perpendicular to the surface. The hydrogen storage mechanism in carbon nanostructures was well described by Cheng.[29] We found that bigger Pd nanoparticles are capable of penetrating into the few-layered graphene surfaces and that smaller Pd nanoparticles are attached to the graphene surface. The nanoholes created by bigger Pd nanoparticles on the graphene surface contain structural defects on the outer surface as well as beneath it. These nanoholes in the graphene surface play a crucial role in hydrogen uptake. H_2 molecules spill over onto the Pd nanoparticles embedded inside the graphene and transform into H atoms, which can migrate to the graphene surface. These H atoms that are now free from the H_2 molecule can adhere to the edges of nanoholes, which contain unsaturated carbons.

CONCLUSION

In summary, we report a facile microwave irradiation method to synthesize a nanohole-structured and palladium-embedded 3D porous graphene. More importantly, we found that Pd nanoparticles were embedded in every nanohole, thus indicating that the Pd nanoparticles are responsible for the creation of the nanoholes on the graphene sheets. The results suggest a substantial rate of interdiffusion of the Pd nanoparticle, which is beneficial for hydrogen storage and CO oxidation. The 3D Pd-E-PG contains nanoholes that provide exceptionally high hydrogen storage and CO oxidation catalytic activity compared with the Pd-D-G. The nanoholes on the graphene surface are responsible for the improved hydrogen storage capability. Finally, we believe that this method will also be useful for fabricating other metal or metal-oxide-porous

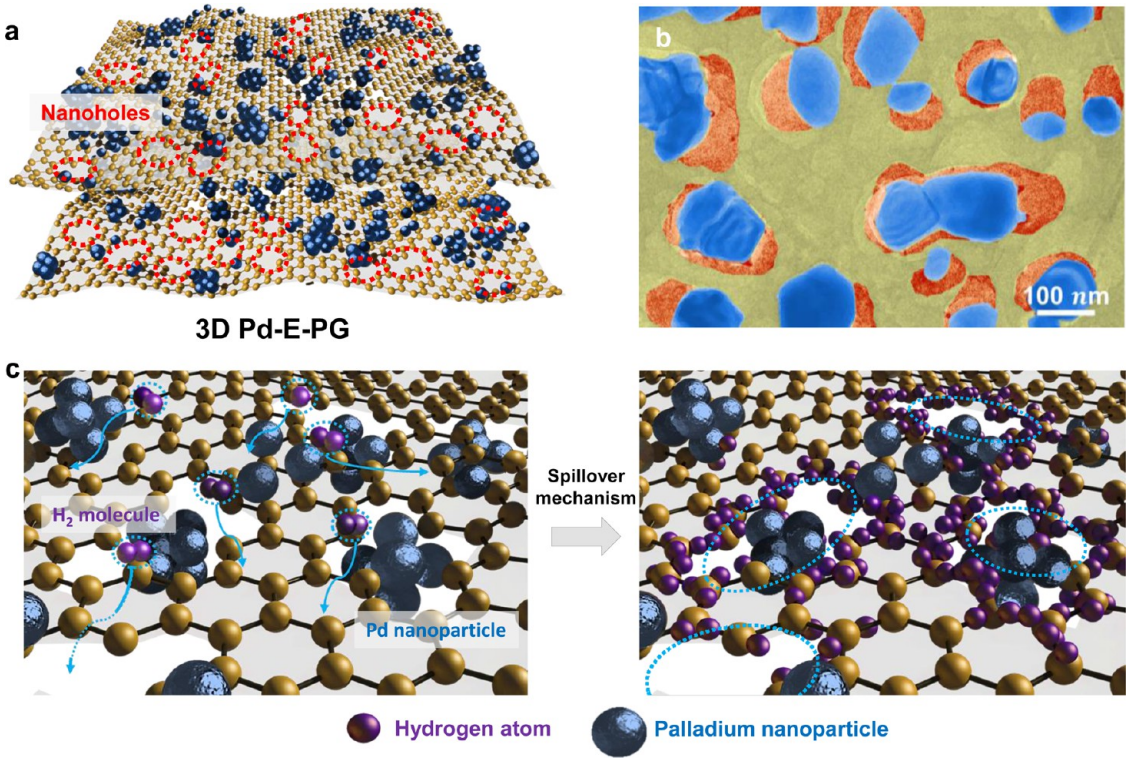

Figure 5. Schematic diagram of spillover mechanism and H_2 storage in the 3D Pd-E-PG containing nanoholes. (a) Illustration of the 3D Pd-E-PG nanoholes. (b) SEM image of the 3D Pd-E-PG with the Pd nanoparticles colored blue. (c) Illustration of the spillover mechanism, including an H atom attached along the nanohole edge.

graphene composites with various applications. This newly acquired understanding of penetration into few-layered graphene can provide a useful guidance for developing generalized methods to produce similar defect-laden nanostructures having multiple functionalities and engineering applications.

MATERIALS AND METHODS

Synthesis. Graphene oxide (GO) was synthesized from natural graphite powder (Merck, 99.99%) using a modified Hummers method.[30] The detailed procedure is shown in the Supporting Information. The growth of the 3D Pd-E-PG nanoholes was carried out in a simple microwave oven, which provides a huge amount of microwave energy in a very short time. First, microwave-exfoliated graphene oxide (10 mg) was sonicated in ethanol with palladium acetate powders (99.99%) (1 mg) for 2 h. After sonication, rigorous stirring for 3 h at room temperature completed the ion exchange between the reduced graphene oxide and the palladium ion precursor. After homogeneous mixing, the mixture was filtered and dried in an oven at 50 °C. Finally, this dried black material was irradiated in a microwave oven at various power intensities for quick exfoliation.

Characterization. The X-ray diffraction patterns of the synthesized hybrid materials were measured using a D/MAX-IIIC (3 kW) (Rigaku) X-ray diffractometer using filtered Cu Kα radiation with an accelerating voltage of 40 kV and current of 200 mA. The sample was scanned at 2θ from 10° to 80°. Field emission scanning electron microscope (FESEM) observations were performed using a Nova NanoSEM 230 FEI at 2 kV in gentle-beam mode without any metal coating and with the fully dried sample loaded on a carbon tape. Elemental analysis was carried out using energy dispersive X-ray spectroscopy (EDS). The EDS analysis was performed at several points in a region, and the data were averaged to obtain representative results. Transmission electron microscopy (TEM) analysis was carried out using a Tecnai G2 F20 microscope operated at 300 kV using a permeable carbon-coated copper grid. The sample was prepared by dispersing a small amount of dry powder in ethanol or water. One droplet of the suspension was then dropped on the carbon-coated, 300-mesh copper TEM grid, and the ethanol was allowed to evaporate in air at room temperature. The Raman spectrum was acquired on a LabRAM HR UV/vis/NIR (Horiba Jobin Yvon, France) using a CW Ar-ion laser (514.5 nm) as the excitation source focused through a confocal microscope (BXFM, Olympus, Japan) equipped with an objective lens (50×, numerical aperture = 0.50) at room temperature. The changes in the surface chemical bonding and surface composition were characterized by FT-IR (Bruker Optiks IFS66 V & Hyperion 3000). The test samples were pressed into tablets with KBr. Hydrogen adsorption with high pressure (up to 80 bar) was measured volumetrically with a computer-controlled commercial pressure−composition isotherm (Belsorp HP). Hydrogen gas (99.9999%) was used in all H_2-sorption measurements. For the PCT measurements, the system was calibrated with $LaNi_5$ at room temperature with activated carbon (surface area ~3000 m^2/g) at 77 K. During the PCT measurement at 77 K, the system was immersed in a liquid-nitrogen Dewar vessel in order to keep the temperature constant at 77 K. Before all measurements, the samples were degassed to a pressure of $(4-8) \times 10^{-7}$ mbar at characteristic temperatures. The oxidation state of the Pd was investigated using X-ray photoelectron spectroscopy (XPS). The XPS spectra were taken using a Thermo VG Scientific Sigma Probe system equipped with an Al Kα X-ray source (1486.3 eV) with an energy resolution of 0.47 eV fwhm under UHV conditions. CO oxidation was performed with the nanocatalyst samples in a flow reactor.[19] Before the reaction, about 50 mg of catalyst was loaded into a quartz tube.

Subsequently, the catalyst was reduced at 250 °C under H_2 flow (5% H_2 in He, a flow of 45 mL min^{-1}) for 30 min and then cooled to room temperature. The reactant gas composition was 4% CO, 10% O_2, and 86% He (balance). The total gas flow rate was 50 mL min^{-1}, controlled by a mass flow controller (Brooks Instrument). CO oxidation was carried out until 100% CO conversion was reached (in the temperature range 150−300 °C). The gas mixture passing through the catalyst powder was analyzed using gas chromatography (DS Science).

Conflict of Interest: The authors declare no competing financial interest.

Acknowledgment. This work was supported by a National Research Foundation of Korea Grant funded by the Korean Government (No. 2012R1A2A2A0104754) and IBS-R004-G4.

Supporting Information Available: The supporting file shows the XPS elemental analysis and BET analysis of the MEGO, Pd-D-G, and 3D Pd-E-PG. The Supporting Information is available free of charge on the ACS Publications website at DOI: 10.1021/acsnano.5b02337.

REFERENCES AND NOTES

1. Cooper, A. I. Porous Materials and Supercritical Fluids. *Adv. Mater.* **2003**, *15*, 1049–1059.
2. Bae, Y. S.; Snurr, R. Q. Development and Evaluation of Porous Materials for Carbon Dioxide Separation and Capture. *Angew. Chem., Int. Ed.* **2011**, *50*, 11586–11596.
3. Lu, A. H.; Schuth, F. Nanocasting: A Versatile Strategy for Creating Nanostructured Porous Materials. *Adv. Mater.* **2006**, *18*, 1793–1805.
4. Yoon, M.; Yang, S. Y.; Wang, E.; Zhang, Z. Y. Charged Fullerenes as High-Capacity Hydrogen Storage Media. *Nano Lett.* **2007**, *7*, 2578–2583.
5. Pupysheva, O. V.; Farajian, A. A.; Yakobson, B. I. Fullerene Nanocage Capacity for Hydrogen Storage. *Nano Lett.* **2008**, *8*, 767–774.
6. Boissiere, C.; Grosso, D.; Chaumonnot, A.; Nicole, L.; Sanchez, C. Aerosol Route to Functional Nanostructured Inorganic and Hybrid Porous Materials. *Adv. Mater.* **2011**, *23*, 599–623.
7. Yildirim, T.; Ciraci, S. Titanium-Decorated Carbon Nanotubes as A Potential High-Capacity Hydrogen Storage Medium. *Phys. Rev. Lett.* **2005**, *94*, 4.
8. Vayssilov, G. N.; Lykhach, Y.; Migani, A.; Staudt, T.; Petrova, G. P.; Tsud, N.; Skala, T.; Bruix, A.; Illas, F.; Prince, K. C.; *et al*. J. Support Nanostructure Noosts Oxygen Rransfer to Catalytically Active Platinum Nanoparticles. *Nat. Mater.* **2011**, *10*, 310–315.
9. Dillon, A. C.; Jones, K. M.; Bekkedahl, T. A.; Kiang, C. H.; Bethune, D. S.; Heben, M. J. Storage of Hydrogen in Single-Walled Carbon Nanotubes. *Nature* **1997**, *386*, 377–379.
10. Beaumont, S. K.; Alayoglu, S.; Specht, C.; Kruse, N.; Somorjai, G. A. A Nanoscale Demonstration of Hydrogen Atom Spillover and Surface Diffusion Across Silica Using The Kinetics of CO_2 Methanation Catalyzed on Spatially Separate Pt and Co Nanoparticles. *Nano Lett.* **2014**, *14*, 4792–4796.
11. Kubas, G. J. Molecular-Hydrogen Complexes - Coordination of a Sigma-Bond to Transition-Metals. *Acc. Chem. Res.* **1988**, *21*, 120–128.
12. Sun, Q.; Wang, Q.; Jena, P.; Kawazoe, Y. Clustering of Ti on a C-60 Surface and Its Effect on Hydrogen Storage. *J. Am. Chem. Soc.* **2005**, *127*, 14582–14583.
13. Li, Y. W.; Yang, R. T. Significantly Enhanced Hydrogen Storage in Metal-Organic Frameworks *via* Spillover. *J. Am. Chem. Soc.* **2006**, *128*, 726–727.
14. Im, J.; Shin, H.; Jang, H.; Kim, H.; Choi, M. Maximizing the Catalytic Function of Hydrogen Spillover in Platinum-Encapsulated Aluminosilicates with Controlled Nanostructures. *Nat. Commun.* **2014**, *5*, 3370.
15. Gadipelli, S.; Guo, Z. X. Graphene-Based Materials: Synthesis and Gas Sorption, Storage and Separation. *Prog. Mater. Sci.* **2015**, *69*, 1–60.
16. Prins, R. Hydrogen Spillover. Facts and Fiction. *Chem. Rev.* **2012**, *112*, 2714–2738.
17. Li, Y. W.; Yang, R. T. Hydrogen Storage in Metal-Organic Frameworks by Bridged Hydrogen Spillover. *J. Am. Chem. Soc.* **2006**, *128*, 8136–8137.
18. Liu, X. M.; Tang, Y.; Xu, E. S.; Fitzgibbons, T. C.; Larsen, G. S.; Gutierrez, H. R.; Tseng, H. H.; Yu, M. S.; Tsao, C. S.; Badding, J. V.; *et al*. Evidence for Ambient-Temperature Reversible Catalytic Hydrogenation in Pt-Doped Carbons. *Nano Lett.* **2013**, *13*, 137–141.
19. Jung, C.-H.; Yun, J.; Qadir, K.; Naik, B.; Yun, J.-Y.; Park, J. Y. Catalytic Activity of Pt/SiO_2 Nanocatalysts Synthesized *via* Ultrasonic Spray Pyrolysis Process under CO Oxidation. *Appl. Catal. B: Environ.* **2014**, *154−155*, 171–176.
20. Kim, S.; Qadir, K.; Jin, S.; Satyanarayana Reddy, A.; Seo, B.; Mun, B. S.; Joo, S. H.; Park, J. Y. Trend of Catalytic Activity of CO Oxidation on Rh and Ru Nanoparticles: Role of Surface Oxide. *Catal. Today* **2012**, *185*, 131–137.
21. Sun, T.; Zhang, Z.; Xiao, J.; Chen, C.; Xiao, F.; Wang, S.; Liu, Y. Facile and Green Synthesis of Palladium Nanoparticles-Graphene-Carbon Nanotube Material with High Catalytic Activity. *Sci. Rep.* **2013**, *3*, 2527.
22. Li, Y.; Fan, X. B.; Qi, J. J.; Ji, J. Y.; Wang, S. L.; Zhang, G. L.; Zhang, F. B. Palladium Nanoparticle-Graphene Hybrids as Active Catalysts for the Suzuki Reaction. *Nano Res.* **2010**, *3*, 429–437.
23. Stankovich, S.; Dikin, D. A.; Piner, R. D.; Kohlhaas, K. A.; Kleinhammes, A.; Jia, Y.; Wu, Y.; Nguyen, S. T.; Ruoff, R. S. Synthesis of Graphene-Based Nanosheets *via* Chemical Reduction of Exfoliated Graphite Oxide. *Carbon* **2007**, *45*, 1558–1565.
24. Banhart, F.; Kotakoski, J.; Krasheninnikov, A. V. Structural Defects in Graphene. *ACS Nano* **2011**, *5*, 26–41.
25. Li, G.; Kobayashi, H.; Taylor, J. M.; Ikeda, R.; Kubota, Y.; Kato, K.; Takata, M.; Yamamoto, T.; Toh, S.; Matsumura, S.; *et al*. Hydrogen Storage in Pd Nanocrystals Covered with a Metal-Organic Framework. *Nat. Mater.* **2014**, *13*, 802–806.
26. Singh, A. K.; Ribas, M. A.; Yakobson, B. I. H-Spillover through the Catalyst Saturation: An Ab Initio Thermodynamics Study. *ACS Nano* **2009**, *3*, 1657–1662.
27. Hu, G.; Nitze, F.; Gracia-Espino, E.; Ma, J.; Barzegar, H. R.; Sharifi, T.; Jia, X.; Shchukarev, A.; Lu, L.; Ma, C.; *et al*. Small Palladium Islands Embedded in Palladium-Tungsten Bimetallic Nanoparticles Form Catalytic Hotspots for Oxygen Reduction. *Nat. Commun.* **2014**, *5*, 5253.
28. Hendriksen, B. L.; Ackermann, M. D.; van Rijn, R.; Stoltz, D.; Popa, I.; Balmes, O.; Resta, A.; Wermeille, D.; Felici, R.; Ferrer, S.; *et al*. The Role of Steps in Surface Catalysis and Reaction Oscillations. *Nat. Chem.* **2010**, *2*, 730–734.
29. Liu, C.; Chen, Y.; Wu, C. Z.; Xu, S. T.; Cheng, H. M. Hydrogen Storage in Carbon Nanotubes Revisited. *Carbon* **2010**, *48*, 452–455.
30. Hummers, W. S.; Offeman, R. E. Preparation of Graphitic Oxide. *J. Am. Chem. Soc.* **1958**, *80*, 1339–1339.